Numerical construction of nonlinear wave-train solutions of the periodic Korteweg–de Vries equation

A. R. Osborne
Istituto di Fisica Generale dell'Università, Via Pietro Giuria 1, Torino 10125, Italy
(Received 12 January 1993)

I discuss a general approach for the numerical construction of exact, nonlinear wave-train solutions to the periodic Korteweg–de Vries (KdV) equation. The method is based upon the periodic inverse scattering transform (IST), a nonlinear generalization of ordinary Fourier series. In this approach, the solution to the KdV equation is represented by a linear superposition of nonlinearly interacting "hyperelliptic functions" which are the nonlinear "oscillation modes" or "degrees of freedom" of the equation; the amplitudes of the nonlinear modes are the constants of the motion for KdV evolution. Using the periodic IST formulation, I numerically construct several low-degree-of-freedom wave trains and discuss some of their physical properties. The approach given here depends explicitly on the application of methods from the field of algebraic geometry. Most of the examples presented are solutions to the KdV equation which have not been previously considered; the solutions are "complex" in the sense that, instead of being a single cnoidal wave, they are "multicnoidal" or "polycnoidal." The IST spectrum often provides a much simpler interpretation of the wave motion than that given by the linear Fourier transform. This occurs primarily because the nonlinear wave trains constructed herein have a small number of IST modes; on the other hand, these wave trains generally require a large number of linear Fourier modes for their description.

PACS number(s): 03.40.Gc

I. INTRODUCTION

The Korteweg–de Vries (KdV) equation is the classical prototypical partial-differential equation for describing long-wave motion in shallow water [1–3],

$$\eta_t + c_0\eta_x + \alpha\eta\eta_x + \beta\eta_{xxx} = 0 \ . \tag{1.1}$$

The surface elevation $\eta(x,t)$ is a function of space x and time t. The constant coefficients are given by $c_0=(gh)^{1/2}$, $\alpha=3c_0/2h$, and $\beta=c_0h^2/6$; g is the acceleration of gravity. Subscripts in (1.1) refer to partial derivatives with respect to x and t; h is the depth. The linearized KdV equation [set $\alpha=0$ in (1.1)] has the dispersion relation $\omega_0=c_0k-\beta k^3$ and c_0 is the associated linear, dispersionless phase speed. Many other applications of the KdV equation are known; these include internal waves [4], Rossby waves [4–6], plasma waves [7], and bores [8].

A rough measure of nonlinearity in a KdV wave train is given by the Ursell number [9]

$$\mathrm{Ur}=\frac{3\eta_0L_0^2}{2h^3}=\lambda\eta_0L_0^2 \ ,$$

where η_0 is a characteristic wave amplitude and L_0 is a characteristic wave length; $\lambda=\alpha/6\beta$. Thus, increasing the amplitude and wavelength and/or decreasing the depth results in an increase in the intrinsic nonlinearity of a wave train.

The periodic cnoidal wave solution to (1.1) is well known,

$$\eta(x,t)=2\eta_c cn^2\{[K(m)/\pi](kx-\omega_c t)|m\}-\bar{\eta} \ . \tag{1.2}$$

The associated dispersion relation has the explicit form

$$\omega_c=\omega_0+c_0k(-\eta_c/h+(k^2h^2/6\pi^2)\{\pi^2-4K(m)[3E(m)-2K(m)]\}) \ , \tag{1.3}$$

where the modulus m of the elliptic function is given by the formula

$$mK^2(m)=(3\pi^2/2k^2h^3)\eta_c \tag{1.4}$$

and $K(m)$, $E(m)$ are complete elliptic integrals of the first and second kind, respectively [10]. The mean of the cnoidal wave over one period, $\bar{\eta}$, is given by

$$\bar{\eta}=(\eta_c/\pi)\int_0^{2\pi}cn^2\{K(m)\theta/\pi;m\}d\theta$$
$$=2\eta_c+4k^2h^3K(m)[E(m)-K(m)]/3\pi^2 \ .$$

This latter expression has been removed from (1.2) to provide consistency with the *spectral description* of the KdV oscillation modes given in Sec. II.

When the modulus $m\to 0$ the cnoidal wave approaches a sinusoid

$$\eta(x,t)=\eta_c\cos(kx-\omega_0t) \ . \tag{1.5}$$

When $m\to 1$ the cnoidal wave approaches the solitary wave solution to KdV,

$$\eta(x,t)=\eta_c \operatorname{sech}^2(\kappa x-\Omega t)\ , \tag{1.6}$$

where $\lambda\eta_c=2\kappa^2$ and the associated dispersion relation is given by $\Omega(\kappa)=\kappa(c_0+4\beta\kappa^2)$.

The Fourier-series representation of the cnoidal wave [10] can be used to recover the Stokes wave for KdV; alternatively a simple Fourier-series expansion in both the wave amplitude $\eta(x,t)$ and dispersion relation $\omega(k)$ [2] also yields Stoke's famous result as applied to the KdV equation,

$$\eta(x,t)=\eta_c\cos\theta+2\eta_c a_c\cos2\theta+2\eta_c a_c^2\cos3\theta+\cdots\ , \tag{1.7}$$

$$\omega=c_0k-\beta k^3+\alpha\eta_c a_c k+\cdots\ , \tag{1.8}$$

where $a_c=3\eta_c/8k^2h^2$, $\theta=kx-\omega_0t$. The dispersion relation (1.8) contains an important dependence on the amplitude which is implicit in all KdV wave trains; a discussion is given in Appendix A for the general case of broad-banded wave trains.

Aside from the above classical results little else was known about the mathematical and physical structure of the KdV equation until more recent developments were obtained during and since the 1960s. Zabusky and Kruskal (ZK) [11] discovered the elegant simplicity of multiple solitary wave interactions by numerical integration of KdV on the spatial periodic domain ($0\le x\le L$; L the period). They found that the shapes of the solitary waves are preserved after collisions, with at most a phase shift resulting from each pairwise interaction. KdV solitary waves were renamed "solitons" by ZK in order to emphasize their particlelike properties. These results lead the way to the subsequent discovery of the *general spectral solution* to the KdV equation on the *infinite line* [$\eta(x,t)\to0$ as $|x|\to\infty$; $-\infty<x<\infty$] by Kruskal and co-workers [12]. The approach, now known as the inverse scattering transform (IST), has since been extended and applied to about 100 nonlinear wave equations [13–17].

The spectral solution to the KdV equation for *periodic boundary conditions* [i.e., $\eta(x,t)=\eta(x+L,t)$, $0\le x\le L$] is also known ([18–22], see also [14] and cited references). IST for infinite-line boundary conditions may be viewed as a nonlinear generalization of the linear Fourier transform [14,16], while for periodic boundary conditions IST is a nonlinear generalization of Fourier series [23–26].

In spite of all the rich mathematical structure now known for the periodic KdV equation, very few specific results are available for the description of complex wave trains or wave fields. Boyd [27–30] and Bobenko and Kubenskii [31] have undertaken a detailed analysis of the simple case with just two nonlinear degrees of freedom. The study of higher degree-of-freedom cases has evidently not been previously undertaken. Here I attempt to address this issue.

A major goal of the present paper is to demonstrate that one can numerically construct complex, nonlinear wave-train solutions to the periodic KdV equation using only a *few IST nonlinear Fourier* degrees of freedom (one to eight in the present study). Wave trains of this type have been found instead to have *many linear Fourier* degrees of freedom. The nonlinear Fourier structure of KdV is here further exploited in order to understand many solutions not easily accessible by direct numerical integration of the equation.

Several aspects of the periodic KdV spectrum have been emphasized by Osborne and Bergamasco [23,24] and Osborne [26,32].

(1) The general solution to the KdV equation with periodic boundary conditions consists of a *linear superposition of hyperelliptic functions* that may be interpreted as a kind of *nonlinear Fourier series* [Eq. (2.1)]. The hyperelliptic functions are referred to as the "μ_j-function oscillation modes" of the periodic KdV equation, which are the natural set of basis functions for *all* solutions of the equation. The $\mu_j(x,t)$ are functions of space and time which reduce to cnoidal waves in the absence of interactions with each other. Normally, however, nonlinear interactions substantially distort the $\mu_j(x,t)$ from the shape of a single cnoidal wave.

(2) The nonlinear Fourier spectral amplitudes (the amplitudes of the hyperelliptic functions or "open bands" in the periodic IST spectrum) are constants of the motion for the periodic KdV equation and hence do not vary in space or in time. This parallels ordinary Fourier analysis, where the Fourier coefficients are space and/or time-independent constants when the wave motion is linear.

(3) The IST nonlinear Fourier series solution to KdV [the linear superposition of the $\mu_j(x,t)$ as given in (2.1)] reduces to a *linear Fourier series* in the small-amplitude limit, where the $\mu_j(x,t)$ decouple and become sine waves [23]. This result reinforces the idea that periodic IST may be viewed as a nonlinear generalization of ordinary Fourier series.

Periodic IST has proven to be an important tool for understanding the original numerical experiments of Zabusky and Kruskal [11], which have been reinterpreted in terms of the nonlinear Fourier approach [24]; in particular, the amplitudes of the solitons and the Fermi-Pasta-Ulam (FPU) recurrence time were verified by periodic theory. Other aspects of this problem, particularly for motion dominated entirely by solitons, have also been studied [25]. More recently Osborne [32] gave a hyperelliptic-function spectral decomposition of the ZK problem using the methods described herein. The analyses entirely corroborate the results given by ZK and provide further insight into the role that solitons and "coherent structures" play in systems with periodic boundary conditions.

While the numerical examples given herein are strictly periodic solutions to the KdV equation, there is absolutely no reason why one should restrict oneself to only periodic solutions. To this end I give a general schematic which classifies *both periodic and quasiperiodic* solutions of the equation. The classification scheme is in terms of the KdV spectrum and hence provides for simple ways to construct all of the periodic and/or quasiperiodic solutions to KdV. These results anticipate many applications which will undoubtedly follow with regard to a whole host of quasiperiodic phenomena, including laboratory and oceanic wave trains [33–35].

Many of the results discussed herein build on the work

of Tracy [36] who first showed how to generate numerical solutions using both the auxiliary variables and the Θ functions of a periodic and/or quasiperiodic soliton equation; he also demonstrated how to force the periodicity condition for the particular case of a modulated plane wave [37,38]. In the present paper I develop a method for forcing periodicity for *all* spectral solutions to the KdV equation.

The remainder of this paper is organized as follows. In Sec. II the nonlinear Fourier-series solution to the KdV equation is summarized. A brief description of the underlying mathematical theory for the periodic KdV spectrum is also given. Section III presents and discusses various examples of complex wave-train solutions to the KdV equation. The appendixes are reserved for a discussion of the numerical methods.

II. THE CONSTRUCTION OF PERIODIC WAVE TRAINS WITH NONLINEAR FOURIER SERIES

A. Overview

The solution to the periodic KdV equation may be written as a linear superposition of nonlinearly interacting, nonlinear waves, referred to as hyperelliptic functions, $\mu_j(x;t)$,

$$\lambda\eta(x,t)=-E_1+2\sum_{j=1}^{N}[\mu_j(x,t)-\bar{\mu}_j] \ . \tag{2.1}$$

Here $\lambda=\alpha/6\beta$ [α and β are physical constants given in the paragraph following (1.1)], and the nonlinear Fourier amplitudes a_j and the means of the hyperelliptic functions $\bar{\mu}_j$ may be specified in terms of a discrete set of eigenvalues $\{E_k\}$ which are $2N+1$ $(1\le k\le 2N+1)$ constants specified in Sec. II B,

$$a_j=\frac{E_{2j+1}-E_{2j}}{2\lambda} \ , \qquad \bar{\mu}_j=\frac{E_{2j}+E_{2j+1}}{2} \ . \tag{2.2}$$

The wave numbers associated with the μ_j for a *periodic* wave train are

$$\mathbf{k}_j=\mathbf{j}\Delta\mathbf{k} \ , \quad \Delta\mathbf{k}=\frac{2\pi}{L} \tag{2.3}$$

for L the period. These are commensurable wave numbers, identical to those for an ordinary Fourier series. As discussed below, *quasiperiodic* wave trains generally do *not* have commensurable wave numbers. The phase of the hyperelliptic functions is governed by specifying the value of the $\mu_j(x=0,t=0)$. In principle, for every set of $\{E_k\}$, one can determine the set of amplitudes a_j and means $\bar{\mu}_j$ [by (2.2)], associated with the wave numbers k_j. Furthermore, given specified amplitudes and commensurable wave numbers $\{a_j,k_j\}$, one can compute the set of eigenvalues $\{E_k\}$ (see the discussion at the end of this section and in Appendix A for numerical details).

Generally speaking the following constraint relation holds:

$$\bar{\mu}_j+a_j<\bar{\mu}_{j+1}-a_{j+1} \ . \tag{2.4}$$

This statement is equivalent to the fact that the eigenvalues in periodic IST are rank ordered,

$$E_{2j+1}>E_{2j} \ . \tag{2.5}$$

As discussed in more detail below the following quantities govern nonlinearity in the periodic KdV equation:

$$\epsilon_j=1/G_j=[\,|\bar{\mu}_{j+1}-a_{j+1}|-|\bar{\mu}_j-a_j|\,]^{-1} \ , \tag{2.6}$$

where the G_j are the "band gaps" in the theory defined by

$$G_j=E_{2j}-E_{2j-1} \ . \tag{2.7}$$

The greater the strength is of the nonlinear interaction between the jth and $(j-1)$th components, the smaller the quantity G_j is. A related nonlinear mode amplitude (an "open band") employed in Appendix A is

$$A_j=E_{2j+1}-E_{2j} \ . \tag{2.8}$$

The interrelationships of the quantities just discussed and the set of eigenvalues $\{E_k\}$ in the periodic IST spectrum are shown schematically in Fig. 1.

The *direct scattering transform* (DST) constitutes the determination of the $\{E_k\}$, the so-called "main spectrum," from some initial wave train $\eta(x,0)$ as discussed in Sec. II B. The *nonlinear Fourier amplitudes* a_j (2.2) are

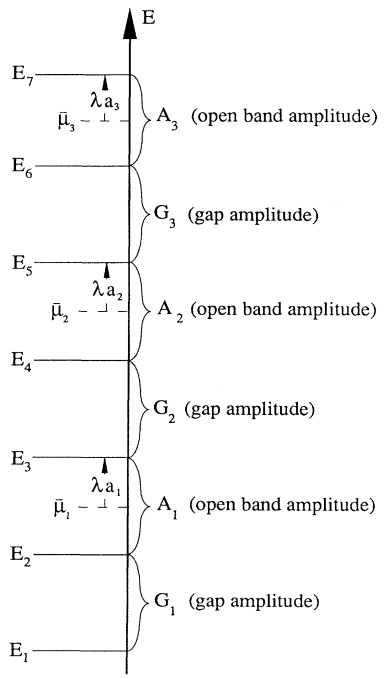

FIG. 1. Schematic of the relationship between certain variables related to the discrete eigenvalues of periodic spectral theory for the KdV equation. Graphed vertically along the E axis are the eigenvalues $\{E_k\}$, $1\le k\le 2N+1$ (which obey the constraint $E_{k+1}>E_k$), the dimensional IST spectra amplitudes a_j, and average hyperelliptic function amplitudes $\bar{\mu}_j$ [Eqs. (2.2)]. The open band amplitudes A_j (2.8) and gap amplitudes G_j (2.7) are also shown.

associated with the wave numbers k_j (2.3). The *inverse scattering transform* constitutes the determination of the hyperelliptic functions $\mu_j(x,0)$ from the set $\{E_k\}$ and the reconstruction of the wave train $\eta(x,0)$ by (2.1). We now discuss some of the details of this formalism.

B. The direct scattering transform

The set of discrete eigenvalues $\{E_k\}$ are constants of the motion for KdV and can be determined directly from a given wave train $\eta(x,0)$. The procedure for a *discrete* wave train [24,26,39] is briefly summarized.

We assume that the continuous function $\eta(x,0)$ is periodic, $\eta(x,0)=\eta(x+L,0)$, and is discretized into M values at small intervals Δx in the spatial variable x; this gives discrete (piecewise constant) amplitudes $\{\eta_m\}$ at coordinate values $\{x_m\}$, $x_m=m\Delta x$, $1\le m\le M$. In order to construct the IST of a wave train on the periodic interval it is convenient to first construct IST on the infinite line. To this end the *spectral matrix* $\mathbf{M}(\kappa)$ is defined for a *localized wave on the infinite line,* i.e., $\eta(x,t)\to 0$ as $|x|\to\infty$ for all t. For a discrete wave train $\mathbf{M}(\kappa)$ is given analytically by

$$\mathbf{M}(\kappa)=\prod_{m=0}^{M}\Delta\mathbf{T}_m(x'_m,\zeta_m,\zeta_{m+1}) , \tag{2.9}$$

where the matrix $\Delta\mathbf{T}_m$ has the form

$$\Delta\mathbf{T}_m(x'_m,\zeta_m,\zeta_{m+1})=\frac{1}{2}\begin{bmatrix}(1+\zeta_{m+1}/\zeta_m)\exp[i(\zeta_{m+1}-\zeta_m)x'_m] & (1-\zeta_{m+1}/\zeta_m)\exp[-i(\zeta_{m+1}+\zeta_m)x'_m]\\ (1-\zeta_{m+1}/\zeta_m)\exp[i(\zeta_{m+1}+\zeta_m)x'_m] & (1+\zeta_{m+1}/\zeta_m)\exp[-i(\zeta_{m+1}-\zeta_m)x'_m]\end{bmatrix} , \tag{2.10}$$

and

$$\zeta_m=[\lambda\eta_m+\kappa^2]^{1/2} , \tag{2.11}$$

$$x'_m=x_m+\Delta x/2 . \tag{2.12}$$

The wave number κ is either real ($\kappa=k/2$, radiation spectrum) or imaginary ($\kappa=iK_n$, the discrete or soliton spectrum, where $1\le n\le N$, N being the number of solitons).

The DST *periodic* spectrum is determined from the so-called *monodromy matrix* $\mathbf{T}$ of periodic theory, which may be computed directly from the infinite-line spectral matrix $\mathbf{M}$ [23,24]. The expression for $\mathbf{T}$ in terms of $\mathbf{M}$ is given by

$$\mathbf{T}(E)=\begin{bmatrix}M_{11}e^{-i\kappa L} & M_{21}e^{-i\kappa L}\\ M_{12}e^{i\kappa L} & M_{22}e^{i\kappa L}\end{bmatrix} . \tag{2.13}$$

It is understood that $\mathbf{M}$ is associated with an *infinite-line* wave train $\eta(x,t)$ which is truncated so as to lie precisely on the interval $(0,L)$ [23,24]. The construction of the nonlinear Fourier spectrum is divided into a "main spectrum" (E_k, $1\le k\le 2N+1$) which is the solution to

$$\{E_j\}:\ \tfrac{1}{2}\mathrm{Tr}\mathbf{T}=\tfrac{1}{2}(T_{11}+T_{22})=\pm 1 \tag{2.14}$$

and an "auxiliary spectrum" [$\mu_j(0,0)$, $\sigma_j=\pm 1$, $1\le j\le N$] which arises as solutions to

$$\begin{aligned}&\{\mu_{j0}\}:\ T_{11}+T_{22}-T_{21}-T_{12}=0 ,\\ &\{\sigma_j\}=\{\mathrm{sgn}[T_{12}+T_{21}]_{E-\mu_j}\} .\end{aligned} \tag{2.15}$$

The mathematical meaning of the σ_j is given below with regard to (2.16).

Procedurally one first computes from an input discrete wave train $\{\eta_m\}$ the monodromy matrix $\mathbf{T}(E)$ [(2.9)–(2.13)] and the trace of the monodromy matrix, $\Delta(E)=\frac{1}{2}\mathrm{Tr}\mathbf{T}(E)$, as a function of $E=\kappa^2$; this allows determination of the *main spectrum* as defined by $\Delta(E)=\pm 1$ (2.14). The $\{E_k\}$ are thus the points of intersection of $\Delta(E)$ with ± 1 and they are numerically found by Newtonian iteration [24,33]. Once the $\{E_k\}$ are known, the nonlinear Fourier amplitudes a_j and wave numbers k_j are computed by (2.2) and (2.3). The *auxiliary* spectrum consists of finding the phases $\mu_j(0,0)$ and the indices σ_j by (2.15). It is worth noting that numerical computation of the monodromy matrix (2.9)–(2.13) requires special consideration as described in detail elsewhere [26,39].

C. The inverse scattering transform

The inverse scattering transform consists of using the $\{E_k\}$ to compute the hyperelliptic functions $\mu_j(x,0)$ [by (2.16)] and to reconstruct the wave train by the linear superposition law (2.1). The functions μ_j evolve in space according to the following system of coupled, nonlinear, ordinary differential equations,

$$\frac{d\mu_j}{dx}=\frac{2i\sigma_j\prod_{k=1}^{2N+1}(\mu_j-E_k)^{1/2}}{\prod_{\substack{k=1\\(k\neq j)}}(\mu_j-\mu_k)} , \tag{2.16}$$

where $1\le j\le N$. The $\sigma_j=\pm 1$ are the signs of the square root of the numerator of (2.16). The μ_j evolve on two-sheeted Riemann surfaces such that the branch points connecting the surfaces correspond to an open band (E_{2j},E_{2j+1}), formed from two adjacent eigenvalues. The μ_j lie in the intervals $E_{2j}\le\mu_j\le E_{2j+1}$ and oscillate between these limits as x is varied. When a μ_j reaches a band edge (i.e., either E_{2j} or E_{2j+1}), the associated σ_j changes sign and the motion leaps to the other Riemann sheet. A numerical procedure for numerically integrating (2.16) is given in [25]. Formally one must specify the eigenvalues $\{E_k\}$, the phases $\{\mu_{j0}=\mu_j(0,0)\}$, and the Riemann sheet indices $\{\sigma_j\}$ in order to integrate (2.16).

The temporal evolution of the μ_j is determined by the following ordinary differential equations (ODE's)

$$\frac{d\mu_j}{dt}=2[-\lambda\eta(x,t)+2\mu_j]\mu_{jx} , \tag{2.17}$$

where $\mu_{jx}=d\mu_j/dx$ is given by (2.16). Note that $\lambda\eta(x,t)$ is defined by the series (2.1) and therefore Eqs. (2.17) are self-contained. It is worth noting that if the right-hand side of (2.17) is written $-c(\mu_j)\mu_{jx}$ for $c(\mu_j)=-2[\lambda\eta(x,t)-2\mu_j]$ then this suggests that the temporal evolution of the μ_j may be viewed as an N-dimensional, nonlinear generalization of the method of characteristics as discussed by Whitham [2].

Solutions to (2.14) and (2.15) constitute the *direct periodic scattering transform.* The construction of the hyperelliptic functions $\mu_j(x,t)$ as solutions of the nonlinear OLE's (2.16) and (2.17) and the determination of solutions of the KdV equation by the superposition formula (2.1) constitute the *inverse periodic scattering transform.* The nonlinear numerical approach given here is completely analogous to linear Fourier series: (1) the nonlinear Fourier spectrum (2.14) and (2.15) gives the amplitudes a_j, phases $\mu_j(0,0)$, and sheet indices σ_j of the KdV oscillation modes in wave-number space and (2) the space-time dynamics of the nonlinear modes $\mu_j(x,t)$ [Eqs. (2.16) and (2.17)] and their linear superposition by a *discrete* version of (2.1),

$$\lambda\eta(x_m,t_0)=-E_1+2\sum_{j=1}^{N}[\mu_j(x_m,t_0)-\bar{\mu}_j] ,$$
$$1\le m\le M \tag{2.18}$$

construct general wave-train solutions to KdV.

In the present application of periodic IST we do not address the time evolution of the motion as given by (2.17). Herein we are interested in constructing wave-train solutions to KdV at a particular fixed time $t=0$. The numerical methods employed for the direct algorithm [(2.14 and 2.15)] are discussed by [24,26,39] and for the inverse problem (2.16) are addressed by [25] and Appendix B. Extension to the temporal evolution of the μ_j as governed by (2.17) is discussed in [32].

D. The single degree-of-freedom solution to KdV

For a single degree of freedom we have $N=1$ and Eqs. (2.1), (2.16), and (2.17) reduce to

$$\frac{d\mu_1}{dx}=[(E_1-\mu_1)(E_2-\mu_1)(E_3-\mu_1)]^{1/2} ,$$
$$\frac{d\mu_1}{dt}=2[-\lambda\eta(x,t)+2\mu_1]\mu_{1x} , \tag{2.19}$$
$$\lambda\eta(x,0)=-\sum_{k=1}^{3}E_k+2\mu_1(x) .$$

The analytical solution of the first two equations of (2.19) is [14]

$$\mu_1=-2(E_2-E_3)cn^2\{\sqrt{E_3-E_1}[x-2(E_1+E_2+E_3)t]+\phi_0|m\}+E_1+E_2 , \tag{2.20}$$

where

$$m=\frac{E_3-E_2}{E_3-E_1} . \tag{2.21}$$

This expression may be compared with the cnoidal wave solution (1.2), i.e., (2.20) is just the KdV spectral representation of (2.1). Note that the spatial period L_1 of μ_1 as $m\to 1$ ($E_1\to E_2$) is given by (Ref. [10], 17.3.26)

$$L_1=\frac{4}{\sqrt{E_3-E_1}}K(m)\cong\frac{16\ln 2+2\ln(E_3-E_1)-2\ln(E_2-E_1)}{\sqrt{E_3-E_1}} . \tag{2.22}$$

It is convenient to think of this formula in the following way. Given E_1,E_2,E_3 let $E_2\to E_1$ for E_1,E_3 fixed, then the spatial period L_1 is dominated by the gap amplitude $G_1=E_2-E_1$. The modulus may then be written as

$$m=\frac{E_3-E_1-G_1}{E_3-E_1} . \tag{2.23}$$

As G_1 is made smaller, $m\to 1$ and the solitary wave solution of KdV is approached. As G_1 is made larger, $m\to 0$ and the solution approaches a sine wave. Thus the parameter G_1 controls both the spatial period and the nonlinearity in this simple example.

An alternative perspective is to rewrite the above results in the following way, explicitly dependent on the wave amplitude A_1 and band gaps G_1 as defined by (2.7) and (2.8)

$$L_1=\frac{4}{\sqrt{A_1+G_1}}K(m)\cong\frac{16\ln 2+2\ln(A_1+G_1)-2\ln(G_1)}{\sqrt{A_1+G_1}} , \tag{2.24}$$

$$m=\frac{A_1}{A_1+G_1} , \tag{2.25}$$

where the associated Ursell number is

$$\mathrm{Ur}=\frac{3A_1L_1^2}{2h^3} . \tag{2.26}$$

These results make clear the dependence of the spatial period L_1 (2.24) and the nonlinearity parameter Ur (2.26) on the nonlinear mode amplitude A_1 and gap width G_1. As $G_1\to 0$ the spatial period $L_1\to\infty$ (logarithmically) and $m\to 1$ which is the solitary wave solution of KdV. In this limit, according to (2.24), G_1 depends on the Ursell number roughly as

$$G_1\sim\exp(-\tfrac{1}{2}\sqrt{\mathrm{Ur}/\lambda}) .$$

The larger the Ursell number is, the smaller G_1 is.

These results are evidently generalizable to the N-band case; this interpretation has been verified in N-band numerical simulations of solitons (see [25]) and in the examples below. Many of these ideas are further exploited in Appendix A to develop a numerical procedure for generating commensurable wave numbers k_j for given specified wave amplitudes A_j.

E. Schematic for interpreting periodic IST spectral theory

In Fig. 2 I give an example of a Floquet diagram, i.e., the trace of the monodromy matrix $\Delta(E)$ is graphed as a function of the squared wave number $E=\kappa^2$, in which the eigenvalues E_k [solutions to $\Delta(E)=\pm 1$] are denoted together with the nonlinear mode amplitudes A_j and gap amplitudes G_j [(2.7) and (2.8)].

Figure 3 gives details of a specific example of the synthesis of a nonlinear wave train for exactly three degrees of freedom. One first constructs the monodromy matrix $\mathbf{T}(E)$ from $\eta(x,0)$ by (2.9)–(2.13) as a function of $E=\kappa^2$. In panel (a) the trace of the monodromy matrix $\Delta=\frac{1}{2}\mathrm{Tr}\mathbf{T}$ is graphed vertically as a function of E. The "main spectrum" consists of the discrete eigenvalues E_k as found from (2.14) together with the phases $\mu_{j0}=\mu_j(0,0)$ and the Riemann sheet indices σ_j from (2.15). The trace $\Delta(E)$ oscillates (crosses zero twice) for each degree of freedom (or oscillation mode) of KdV. When $\Delta(E)$ stops or "turns around" at either $+1$ or -1 the oscillation mode has zero amplitude because $E_{2j}=E_{2j+1}$ [see (2.2)]. On the other hand, when $\Delta(E)$ moves to the right of -1 or the left of $+1$ a finite amplitude oscillation mode occurs because $E_{2j}\neq E_{2j+1}$; in the present example the modes for $j=5$, 8, and 12 are seen to have finite amplitude; all other modes are "degenerate" ($E_{2j}=E_{2j+1}$) and therefore have zero amplitude. The finite-amplitude modes (the "open bands" in the spectrum) correspond to the shaded regions in panels (a) and (b). The hyperelliptic oscillation modes, $\mu_5(x,0)$, $\mu_8(x,0)$, and $\mu_{12}(x,0)$ are graphed [by numerical integration of (2.16)] inside the shaded regions in panel (b). For the present case it can be seen that the modes are quite distorted from the shape of a simple sinusoid, even for this mildly nonlinear case. The linear superposition of these modes via (2.1) gives the solution to the KdV equation [Fig. 3(c)].

In the above example it would indeed be fortuitous to determine the IST spectrum of some wave train and to find exactly three degrees of freedom. On the other hand, it would be quite useful to have a procedure for constructing wave trains with exactly N degrees of freedom. To this end I consider a nontrivial variation of the above procedure which I use herein to synthesize nonlinear wave trains, i.e., N band *periodic* solutions to KdV are constructed by selecting specific values for the nonlinear oscillation mode amplitudes a_j, phases $\mu_j(0,0)$, and commensurable wave numbers $k_j=2\pi j/L$. From these the E_k are constructed via numerical implementation of the Jacobian transformation of algebraic geometry (see Appendix A). Then the oscillation modes $\mu_j(x,0)$ are found numerically by the integration of Eq. (2.16) (Appendix B) and the solution to KdV is found by linear superposition (2.1). It is worth noting that summing over only a subset of the N terms in (2.1) (ostensibly to observe either the solitons or the radiation spectrum in the absence of interactions with the other components) is referred to as *nonlinear filtering* [24,32,36].

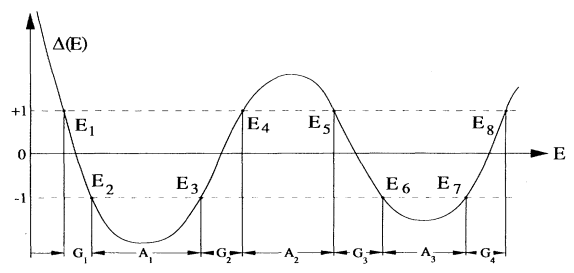

FIG. 2. Example Floquet diagram $\Delta(E)$ vs E, together with the "main spectrum" eigenvalues $\{E_k\}$, the hyperelliptic function amplitudes $\{A_k\}$, and band-gap amplitudes $\{G_j\}$.

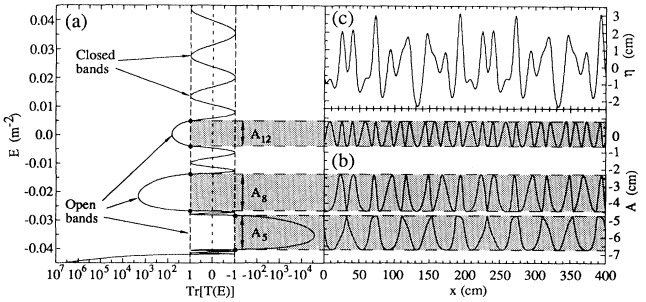

FIG. 3. Schematic for the synthesis of a periodic KdV wave train using the periodic inverse scattering transform. (a) Floquet spectrum with "open bands" denoted by shaded regions. (b) Nonlinear (hyperelliptic) oscillation modes of KdV. (c) Complex wave-train solution to KdV. The linear superposition (2.1) of these (decidedly nonsinusoidal) modes give the solution to KdV in (c).

F. Various approaches for constructing wave trains

Figure 4 gives a schematic of various possibilities for synthesizing wave trains of KdV using the formulation of the periodic and/or quasiperiodic inverse scattering transform. Four methods are given for the specification of the KdV spectrum, i.e., the eigenvalues $\{E_k\}$, phases $\{\mu_j(0,0)\}$, and Riemann sheet indices σ_j, from which specific wave trains may be synthesized. The hyperelliptic oscillation modes are then computed numerically by (2.16) and their linear superposition gives the solution to KdV by (2.1) [or more accurately the discrete counterpart (2.18)]. Each approach is labeled by a number 1–4 in Fig. 4. Approaches 1 and 2 compute hyperelliptic functions $\mu_j(x,0)$ which are quasiperiodic, while approaches 3 and 4 generate hyperelliptic functions which are instead periodic. In approach 1 one arbitrarily selects the set $\{E_j,\mu_j(0,0),\sigma_j\}$ (while obeying the ordering constraint $E_{2j+1}>E_{2j}$); since the choice of the $\{E_k\}$ is arbitrary, there is no guarantee that the wave numbers k_j are commensurable, and so in general this approach gives quasiperiodic μ_j. It then follows that the wave-train solution to KdV (2.1) is also quasiperiodic for approach 1.

An alternative method is given by approach 2 where the nonlinear mode amplitudes and average values $\{a_j,\bar{\mu}_j\}$ are chosen instead of the $\{E_j\}$. In this case the $\{E_j\}$ are subsequently computed by (2.2). It is clear that approach 2 also yields quasiperiodic wave trains since,

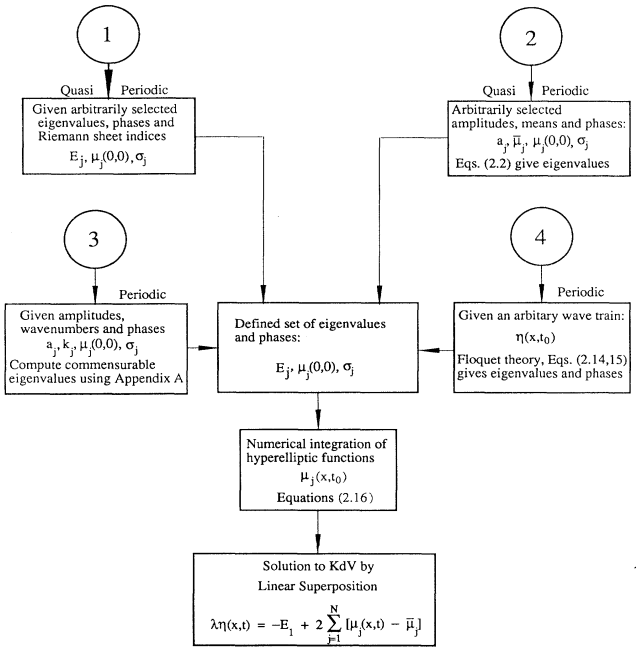

FIG. 4. Schematic of approaches for generating complex wave-train solutions to the KdV equation. The following constraints must hold in the selection of the phases and eigenvalues: (a) $E_{2j+1} > E_{2j}$ and (b) $E_{2j+1} \leq \mu_j(0,0) \leq E_{2j}$.

once again, the selection of the eigenvalues $\{E_k\}$ is arbitrary.

A peripherally related approach would be to choose the set $\{A_j, G_j\}$ and then to subsequently compute the $\{E_j\}$ by Eqs. (2.7) and (2.8). Once again, due to the arbitrariness of the selection procedure, these KdV solutions are also clearly quasiperiodic. However, this approach, seemingly a simple extension of the above two methods, is nevertheless particularly important because it leads directly to approach 3. It is with this latter method that the *periodic* wave trains presented in the present paper have been generated via the procedure in Appendix A. In this case one provides the set of amplitudes, wave numbers, phases, and sheet indices $\{a_j, k_j, \mu_j(0,0), \sigma_j\}$ and then the approach in Appendix A is applied to compute the eigenvalues $\{E_k\}$ in such a way as to guarantee that the IST wave numbers K_j [see Eq. (A4) in Appendix A] are *commensurable*. One first computes the $\{A_j\} = 2\lambda\{a_j\}$ and makes estimates for the "starting values" of the $\{G_j\}$. One then iterates on the G_j to compute a "commensurable set" of the $\{E_k\}$ to ensure that the $\mu_j(x,0)$ are periodic and consequently the computed wave train $\eta(x,0)$ is also periodic. This procedure may be somewhat technical to those unfamiliar with the methods of algebraic geometry and the details have been deferred to Appendix A.

Finally in approach 4 one provides as input an *arbitrary wave train* $\eta(x,0)$ which is assumed to be periodic on $(0 \leq x \leq L)$. Floquet theory, as represented by (2.14) and (2.15) automatically gives eigenvalues $\{E_k\}$ with associated commensurable wave numbers k_j, phases $\mu_j(0,0)$ and sheet indices σ_j. This method therefore yields periodic functions $\mu_j(x,0)$ and hence the reconstructed solution to KdV via (2.1) is also periodic.

It is worthwhile noting that the spirit of the work given here is based upon the following idea: One specifies the band edges and the initial conditions of the auxiliary variables and then solves for the x (and possibly t) dynamics of the auxiliary variables. This procedure works for the KdV equation, but it is also known *not* to work for the nonlinear Schrödinger equation, another soliton system. This is because in the latter case one must choose the initial conditions of the auxiliary variables subject to a constraint. No such constraint exists for the KdV equation [20]. Future applications of the methods given herein to other soliton wave equations will require consideration of constraints of this type; in this regard the work of Tracy is of considerable importance [37,38].

III. EXAMPLES OF NONLINEARLY SYNTHESIZED WAVE TRAINS

I now give a number of examples of numerically constructed KdV wave trains which have from one to eight degrees of freedom. The wave trains have been selected to provide some insight into the nonlinear Fourier structure of the KdV equation. The examples are dimensional, with wave-train amplitudes $\eta(x,0)$ given in centimeters; the water depth h is taken to be 5 cm in all cases. The hyperelliptic function amplitudes are also graphed dimensionally; to this end, in this section, we write the dimensional expressions

$$E_k' = E_k/\lambda\ ,$$
$$\mu_j' = 2\mu_j(x,0)/\lambda\ , \tag{3.1}$$
$$\bar{\mu}_j' = 2\bar{\mu}_j(x,0)/\lambda\ .$$

Here E_k', μ_j', and $\bar{\mu}_j'$ have dimensions in centimeters. The linear superposition law (2.1), in dimensional form, reads (upon dropping the primes)

$$\eta(x,t) = -E_1 + \sum_{j=1}^{N}[\mu_j(x,t) - \bar{\mu}_j]\ . \tag{3.2}$$

The examples which follow refer to dimensional variables as defined by (3.1) and (3.2).

A. One degree of freedom

A single-degree-of-freedom solution of the periodic KdV equation (2.19) and (2.20), e.g., the classical cnoidal wave, is shown in Fig. 5(a). The lower curve shows the hyperelliptic function $\mu_1(x,0)$ as it evolves within the limits of its open band (represented by the horizontal dashed lines); the upper curve (for the one-degree-of-freedom example given here) is the solution to the KdV equation, $\eta(x,0)$, which is identical to the single $\mu_1(x,0)$ [compare the last of Eq. (2.19) with (2.20)]. Floquet eigenvalues have been chosen [via (2.20)] to give a wave amplitude of 2.5 cm and a spatial period of 33.33 cm. The Fourier transform of the wave form is shown in Fig. 5(b). Note the large number of non-negligible components, particu-

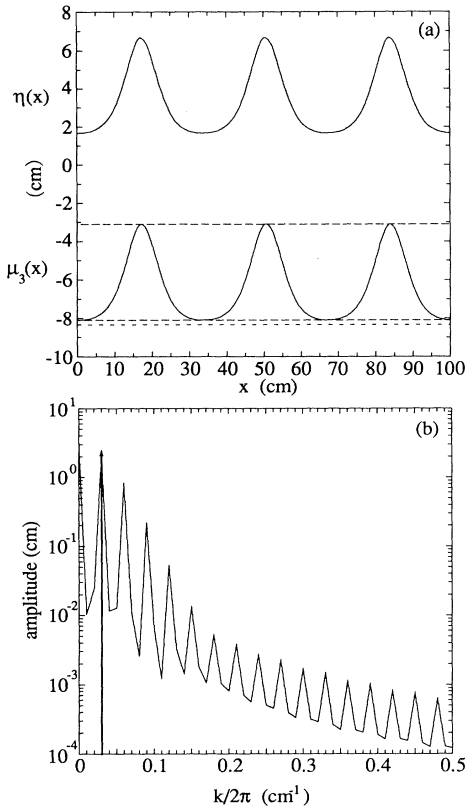

FIG. 5. A single-band periodic KdV solution, the classical cnoidal wave (a). The linear Fourier transform of the cnoidal wave train and its scattering transform (vertical arrow) (b).

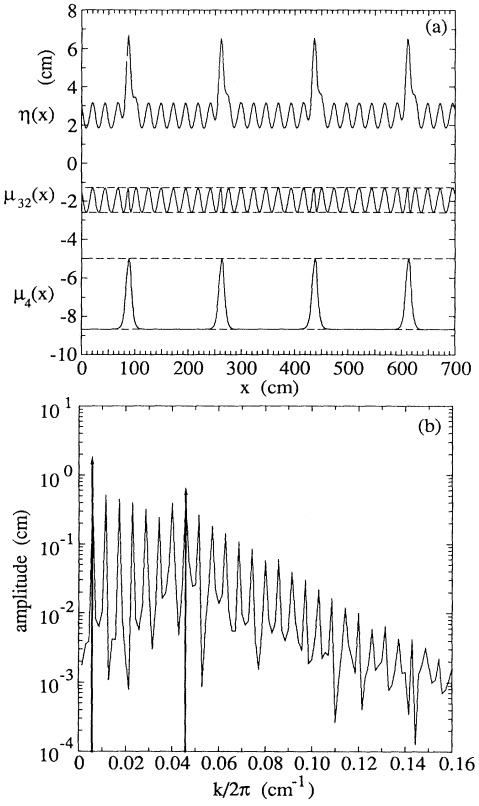

FIG. 6. A synthesized two-band spatially periodic KdV wave train: nonlinear superposition of a soliton and sine wave (a). The linear Fourier transform of the wave train and its scattering transform (vertical arrows) are shown in (b).

larly large-amplitude harmonics, in the Fourier spectrum. In Fig. 5(b) the KdV IST spectrum is also shown (vertical arrow); this represents the single cnoidal wave component. The scattering transform spectrum is seen to be considerably simpler than the linear Fourier transform for this simplest of examples.

B. Soliton plus a sine wave

The nonlinear superposition of a soliton and a sine wave is shown in Fig. 6. The soliton might more accurately be described as a "soliton train" because the soliton pulse is repeated four times within the selected period of $L=700$ cm shown in the figure. Formally each of the two modes in this example, in the absence of the other, is a cnoidal wave. For the soliton the modulus m is near to but slightly less than 1. Since a single pulse of the wave train is graphically indistinguishable from a soliton on the infinite interval, we refer to this wave as a soliton train of period four [the curve labeled $\mu_4(x)$ in Fig. 6] (see the paper by Ferguson, Flaschka, and McLaughlin [40] for a fundamental discussion of solitons and soliton trains for periodic boundary conditions). Generally speaking the nonlinearity and spatial periodicity of the nonlinear modes are governed by the value of G_j as discussed with regard to (2.6). In this example for G_j small, one finds a soliton train while for G_j large, one has a sine wave. The "sine wave" has wave number $k_j=2\pi j/L$ for $j=32$ and is labeled μ_{32} in Fig. 6. Note that nonlinear interactions with the soliton train distort the sine wave, e.g., there is a spatial compression of the sine wave that coincides with the occurrence of each pulse in the soliton train. The compression may be interpreted as a "phase shift" of the sine wave in the vicinity of the soliton (phase shifting in the context of periodic IST is further discussed in Refs. [24,32]). The solution $\eta(x,0)$ to the KdV equation (linear superposition of μ_4 and μ_{32}) is shown in the upper graph of Fig. 6(a). The peaks of the soliton train clearly emerge above the low-amplitude sine wave. The DST spectrum (two vertical arrows) and the linear Fourier transform are shown in Fig. 6(b). For this example the number of Fourier modes is again quite large compared to the number of scattering transform modes.

C. A nonlinear beat: two closely spaced nonlinear oscillation modes

It is well known that a linear beat is the linear superposition of the two sine waves whose wave numbers (k_1,k_2) differ by a small amount Δk,

$$\Delta k=k_2-k_1\ ,\quad \bar{k}=\tfrac{1}{2}(k_1+k_2)\ ,$$

where $\bar{k}$ is the "dominant" wave number. Figure 7 shows the generalization of this idea to a nonlinear beat for the

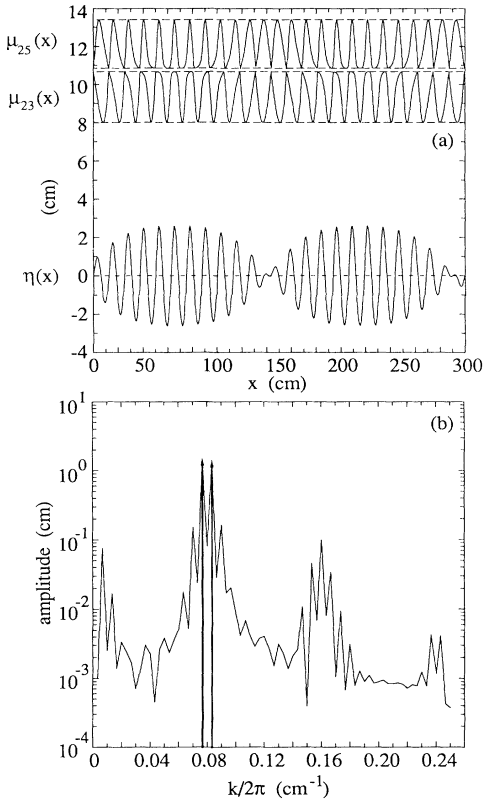

FIG. 7. A two-band solution to KdV corresponding to a nonlinear beat (a). The linear Fourier transform of the wave train and its scattering transform (vertical arrows) are shown in (b).

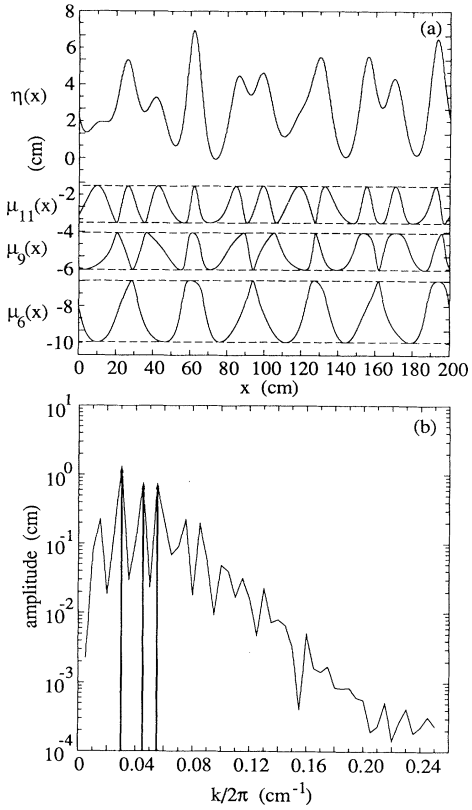

FIG. 8. A synthesized three-band spatially periodic KdV wave train (a). The linear Fourier transform of the wave train and its scattering transform (vertical arrows) are shown in (b).

KdV equation. Two closely spaced nonlinear modes [$\mu_{23}(x)$ and $\mu_{25}(x)$] are shown in panel (a) of the figure. It is worth noting that, in spite of the distorted nonsinusoidal shape of the two nonlinear modes in Fig. 7(a), the resultant beat is nevertheless quite regular in appearance. The two components of the IST spectrum (vertical arrows) are shown in Fig. 7(b) together with the linear Fourier transform. The latter is seen to be rather complex with a central peak near the two IST modes; higher harmonics as well as low wave-number components (radiation stress) are also present. This example illustrates once again how a simple scattering transform spectrum may require a complex linear Fourier spectrum for its description.

D. Three degrees of freedom

The example of a synthesized three-band, spatially periodic KdV wave train [Fig. 8(a)] is now considered. The three lowermost curves show the hyperelliptic functions $\mu_1(x,0)$, $\mu_2(x,0)$, and $\mu_3(x,0)$ oscillating in their respective open bands (represented by the horizontal dashed lines); the uppermost curve depicts the wave train $\eta(x,0)$, which is the sum of the three finite amplitude $\mu_j(x,0)$. The amplitudes of the μ_j are, respectively, 2.5, 1.5, and 1.5 cm, and the Floquet eigenvalues were chosen (see Appendix A) to give commensurable wave numbers $k_j = 2\pi j/L$ for $j = 6$, 9, and 11 over the spatial period of 200 cm. Note that the shapes of the components deviate substantially from cnoidal waves. The Fourier transform of the wave train is given in Fig. 8(b) and is to be contrasted to the scattering transform (vertical arrows). As in the previous examples the Fourier transform has a spectrum which is quite complex compared to the KdV oscillation modes.

E. Five degrees of freedom

In Fig. 9 is an example of a synthesized wave train with five modes. The five lowermost curves show $\mu_{1-5}(x,0)$; the uppermost curve depicts the wave train $\eta(x,0)$ resulting from the linear superposition of the $\mu_j(x,0)$. The amplitudes of the μ_j components are, respectively, 1.5, 0.666 66, 0.5, 0.333 33, and 1.5 cm, and the Floquet eigenvalues were determined (see Appendix A) to ensure commensurable wave numbers k_j with indices $j = 5$, 7, 9, 10, and 11 within the spatial period of 200 cm. Only the uppermost component resembles a cnoidal wave; the others are instead quite deformed from this familiar shape (compare to Fig. 5). The μ_j-function oscillation modes are clearly nontrivial generalizations of the ordinary linear Fourier (sinusoidal) modes. Figure 9(b) shows the Fourier transform of the wave train and the scattering transform is given by the five vertical arrows. The linear Fourier transform is again seen to be much more complex than the scattering transform representation.

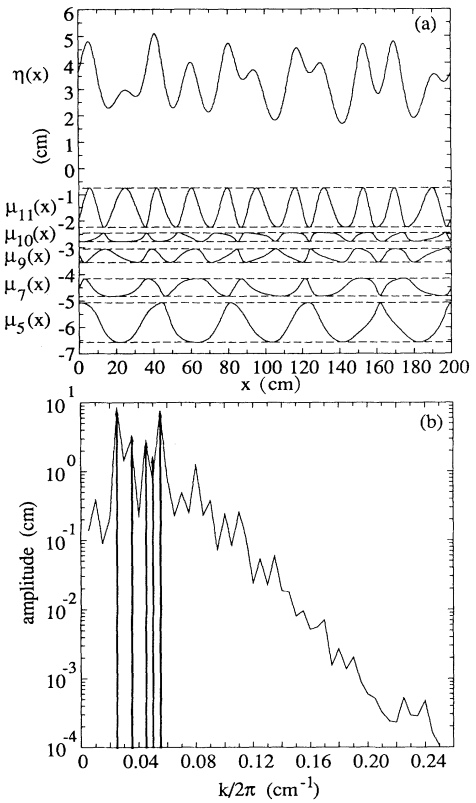

FIG. 9. A synthesized five-band spatially periodic KdV wave train (a). The linear Fourier transform of the wave train and its scattering transform (vertical arrows) are shown in (b).

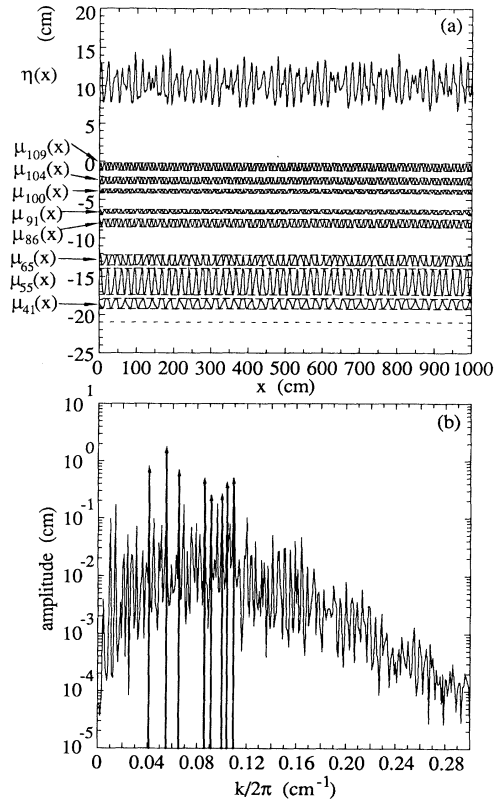

FIG. 10. A synthesized eight-band spatially periodic KdV wave train (a). The linear Fourier transform of the wave train and its scattering transform (vertical arrows) are shown in (b).

F. Eight degrees of freedom

The example of a synthesized eight-band, spatially periodic KdV wave train is shown in Fig. 10. The eight lowermost curves are the $\mu_{1-8}(x,0)$, while the uppermost curve depicts the KdV wave train $\eta(x,0)$. The μ_j have been plotted dimensionally with amplitudes given by 4.3333, 3.5, 1.3333, 1.0, 0.5, 0.5, 0.8333, and 1.0 cm, while the Floquet eigenvalues $\{E_k\}$ were chosen to give commensurable wave numbers k_j with indices $j=41$, 55, 65, 86, 91, 100, 104, and 109 over the selected spatial period of 1000 cm. In Fig. 10(b) the Fourier transform of the wave form is given together with the scattering transform, which is represented by the vertical arrows. The Fourier transform is rather broad banded, while the KdV spectrum has exactly eight components.

IV. SUMMARY AND CONCLUSIONS

Generally speaking, many of the features of linear Fourier analysis are preserved in the periodic IST formulation for KdV given herein. In effect one invokes procedure 3 of Fig. 4, and the selected amplitudes, wave numbers, and phases are all that are necessary to construct a periodic wave train by numerical integration of the ODE's (2.16). The amplitudes and wave numbers are those already familiar to us from linear Fourier theory, but the phase information is more complex as it is contained both in the $\mu_j(0,0)$ and the Riemann sheet indices σ_j [23]. Generally speaking, solutions to KdV in the μ representation consist of the linear superposition of the nonlinear oscillation modes: nonlinear interactions are manifested as distortions of these modes from the familiar shape of the cnoidal wave. We find, for the cases considered herein, that many linear Fourier modes are required to describe a KdV wave train which has instead only a few IST components. However, it is worthwhile keeping in mind that the full picture of wave motion described by KdV is much more complex. This is because the KdV mode amplitudes are generally constants of the motion, while the linear Fourier amplitudes are functions of both space and time for nonlinear evolution governed by KdV.

Therefore, an additional important question is: What happens during the time evolution of a KdV wave train? Since the KdV mode amplitudes are constants independent of space and time, the nonlinear Fourier representation maintains its simple picture, even during time evolution, although the *physical shape* of the KdV modes may change with time [25,32]. Recent laboratory experiments substantiate these conclusions [35], e.g., laboratory-generated shallow-water surface waves are found to have KdV mode amplitudes which are essentially constants in space and time, while the linear Fourier amplitudes are instead strongly dependent on space and time.

The example wave trains considered herein are rela-

tively simple, but I have not considered soliton interactions in detail, a topic covered elsewhere [24,25,32]. N-soliton solutions to (2.16) are difficult to compute numerically due to the presence of large nonlinear interactions. Except for the case of only one soliton in the IST spectrum, no individual μ_j function can represent a soliton. We know of course the theoretical structure of KdV allows for the linear superposition of N $\mu_j(x,0)$ as a representation of the interaction of exactly N solitons [24]. Since soliton interactions are highly nonlinear, it is clear from the outset that the μ_j functions cannot themselves generally be solitons (since the μ_j obey a linear superposition law while solitons do not). In this case the $\mu_j(x,0)$ and their ODE's (2.16) are "nearly singular" in the sense discussed in Ref. [25]. The μ_j in two adjacent bands, because they undergo nonlinear interactions while simultaneously obeying a linear superposition law, are *phase locked* with each other and actually reach and touch the band edges at the same instant of their evolution.

The phase locking often seen among the IST components suggests that the random-phase approximation, commonly employed in linear stochastic representations of ocean waves, is evidently not appropriate for the evolution of nonlinear wave trains for KdV. In view of recent results applying periodic IST in the analysis of oceanic internal waves [33], surface waves [34], and laboratory-generated shallow water waves [35], evidently the search for nonlinear stochastic representations of complex nonlinear surface wave trains presents open, interesting and challenging problems.

ACKNOWLEDGMENTS

We acknowledge valuable aid and encouragement from Professor L. Bergamasco. E. Segre provided graphical assistance. This work was supported in part by the U.S. Office of Naval Research (ONR Grant No. N00014-92-J-1330) and by the Progetto Salvaguardia di Venezia del Consiglio Nazionale delle Ricerche, Italy.

APPENDIX A: PERIODIC KdV WAVE TRAINS: COMPUTATION OF COMMENSURABLE WAVE NUMBERS

This appendix briefly describes the procedure (see Fig. 11) that allows for the construction of a *periodic* KdV wave train for a specific number N of nonlinear harmonic modes. The method is used to compute the examples of periodic wave trains given in the present paper. The periodicity condition implies that the wave numbers be commensurable as given in (2.3). Since, generally speaking, spectral theory for KdV wave trains is quasiperiodic, the periodicity condition must be viewed as exceptional. As seen below, specification of commensurable wave numbers by (2.3) and a subsequent determination of the associated main spectrum $\{E_j\}$ is an interesting mathematical and numerical task. Many of the results are beyond the scope of this paper and only the basic principles are outlined here; details are given elsewhere [32]. The procedure given in this appendix is referred to as "approach 3" in Fig. 4. Schematics of the variable definitions are given in Figs. 1–3.

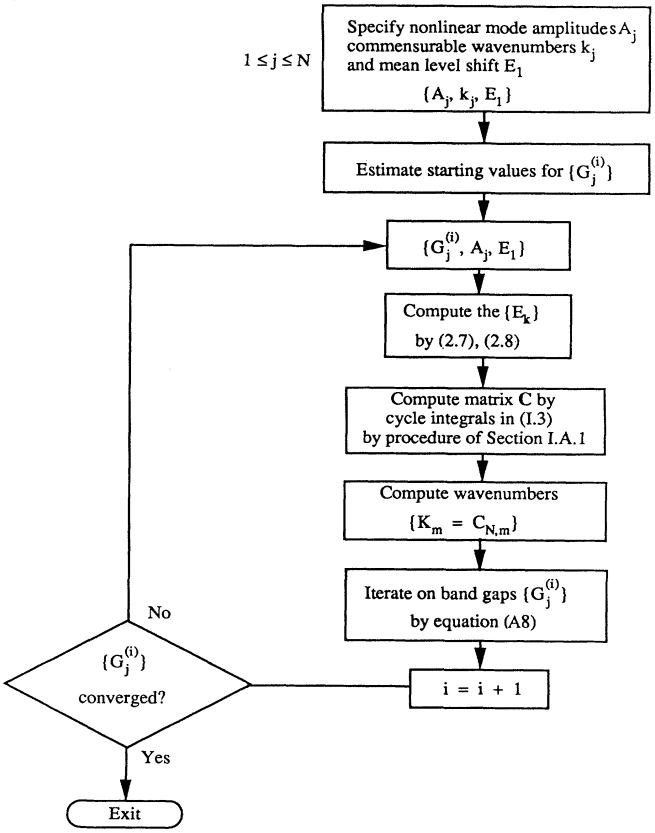

FIG. 11. Procedure described in Appendix A for computing commensurable wave numbers. The approach ensures that wave trains constructed by the methods given herein are periodic (rather than quasiperiodic) functions of the spatial variable x. Note that the flow chart needs to be iterated over all j ($1 \le j \le N$) to include all the degrees of freedom.

It is well known that the dynamical motion of the μ_j functions, as governed by (2.16) and (2.17), may be linearized by means of a Jacobian transformation, which is a particular case of an Abel mapping (see, for example, [14,16] and references cited therein). The linearizing Jacobian transformation maps the μ representation $\{(\mu_j(x,t),\sigma_j)\}$ (which evolves *nonlinearly* in space and time) to new variables $\{\zeta_m(x,t)\}$ (which evolve *linearly* in space time). The solution $u(x,t)$ of the dimensionless KdV equation

$$u_5 + 6uu_t + u_{xxx} = 0$$

is then expressed in terms of the variables ζ_m by means of generalized Θ functions [41]

$$u(x,t) = 2\frac{\partial^2}{\partial x^2} \ln\Theta(\zeta_1, \ldots, \zeta_N) + \text{const} . \tag{A1}$$

The new variables ζ_m depend linearly on x and t in the following way:

$$\zeta_m(x,t) = K_m x - \omega_m t + \eta_{0m} , \tag{A2}$$

in which ζ_{0m} are constants given elsewhere [32], and the K_m and ω_m are the wave numbers and frequencies associated with the matrix coefficients C_{jm} which are computed uniquely from the set of eigenvalues $\{E_k\}$ by solving (see [14])

$$\mathbf{C}=\{C_{jm}\}=\frac{1}{2\pi}\left[\oint_{\alpha_j}\frac{E^{m-1}}{\left[\prod_{k=1}^{2N+1}(E-E_k)\right]^{1/2}}dE\right]^{-1} . \tag{A3}$$

Here $\{\alpha_j\}$ is a canonical set of closed paths (contours or "cycles" as they are referred to in algebraic geometry) surrounding each one of the N forbidden bands. The matrix $\mathbf{C}$ is square since $1\le m\le N$ and $1\le j\le N$. Explicitly, one finds for the wave number and frequency in terms of the matrix elements $\{C_{jm}\}$ and eigenvalues $\{E_k\}$

$$\begin{aligned} K_m &= C_{N,m} , \\ \omega_m &= 8C_{N-1,m}+4C_{N,m}\sum_{k=1}^{2N+1}E_k . \end{aligned} \tag{A4}$$

The second equation of (A4) is the *generalized dispersion relation* for complex KdV wave trains [in the case $N=1$ one has $K_1=C_{1,1}$ and $\omega_1=4\ (E_1+E_2+E_3)C_{1,1}$; see (2.20) for the dimensional form of ω_1]. It should be clear that the wave numbers and frequencies $\{K_j,\omega_j\}$ of the Θ functions apply also to the μ_j representation. It is in this sense that I now provide numerical methods to compute the (K_j,ω_j) in such a way as to force commensurability of the K_j [i.e., to require that $K_j=k_j$ as in (2.3)] and hence to ensure spatial periodicity of KdV wave trains in the μ representation.

Generally speaking $K_jL=2\pi n_j$, so K_j is also the wave number for the μ_j, in the sense that $K_jL/2\pi$ indicates how many times each μ_j oscillates while evolving from x to $x+L$ in such a way that the index σ_j changes signs K_jL/π times. This implies that each μ_j oscillates n_j times within the period L, but does not necessarily mean that each μ_j is periodic with period L/n_j unless specific conditions are met to ensure periodicity (commensurability of the wave numbers K_j) as discussed below. In fact, developing methods for ensuring periodicity of the μ_j is the goal of this appendix.

1. Computing the wave numbers and frequencies $\{K_j,\omega_j\}$ from the eigenvalues $\{E_k\}$

The mapping $\{E_k\}\to\{K_j,\omega_j\}$ implies that, given the set $\{E_k\}$, the quantities K_j and ω_j in (A4) are obtained by calculating the matrix of integrals in (A3), inverting the matrix, and then summing the prescribed elements in (A4). The most difficult steps are the computation of the cyclic integrals in (A3) and the inversion of the $N\times N$ matrix to obtain C. The (K_j,ω_j) are then easily computed via (A4). Numerical computation of the cycle integrals is now discussed in detail.

Calculation of the cycle integrals

To numerically evaluate the integrals of (A3) I deform the integration contour, make a simple change of variables, and use a standard variable-step fourth-order integration scheme incorporating simultaneous implementation of both Runge-Kutta and Adams-Moulton integration algorithms [42]. The specific steps are as follows.

(a) *Deformation of the contours.* The argument of the integrals (A3) is, for every value of the index m, an analytical function $f_m(E)$ defined on the Riemann surface Γ, e.g., over the "cycles" or contour integrals α_j surrounding adjacent eigenvalues of an open band (E_{2j},E_{2j+1}). The points $E=E_k$ $(k=1,\ldots,2N+1)$ are polydromy points at which the integrand goes to ∞, and the point $E=\infty$ is an extra polydromy point with value 0. The integration path α_j crosses the real E axis twice, so that a change of the Riemann sheet has to be taken into account. Note that due to the analyticity of the function $f_m(E)$ the contour can be contracted so that it is infinitesimally close to the open band $[E_{2j},E_{2j+1}]$ on the real axis; this gives an integration path symmetrical about the segment and hence the small loops around the branch points E_{2j} and E_{2j+1} tend to cancel each other. The change of Riemann sheet involves the change of sign of the radical in the denominator of $f_m(E)$ and it is clear that $f_m(E\in$(upper part of the cycle)$)=-f_m^*(E^*\in$(lower part of the cycle)$)$. It then follows that

$$\begin{aligned} \oint_{\alpha_j}f_m(E)dE &= 2\int_{E_{2j}}^{E_{2j+1}}\mathrm{Re}(f_m(E))dE \\ &= 2\int_{E_{2j}}^{E_{2j+1}}f_m(E)dE , \end{aligned} \tag{A5}$$

where the two halves of the integration cycle are made in opposite directions. This last integral is defined in the Riemann sense, because the integrand $f_m(E)$ goes to infinity at the integration limits as $(E-E_{2j})^{-1/2}$ and $(E-E_{2j+1})^{-1/2}$, but the integral nevertheless converges.

(b) *Change of integration variable.* The above form is not yet suitable for numerical integration because the integrand approaches infinity at the branch points. This difficulty is overcome with the aid of a simple change of variables. For numerical purposes the divergence of the integrand at $E=E_k$ can be overcome by setting [23]

$$\begin{aligned} E(z) &= \frac{E_{2j+1}-E_{2j}}{2}\cos(z)+\frac{E_{2j+1}+E_{2j}}{2} \\ &= \lambda a_j\cos(z)+\bar{\mu}_j \end{aligned} \tag{A6}$$

in the cycle integrals

$$\begin{aligned} &\oint_{\alpha_j}\frac{E^{m-1}}{\left[\prod_{k=1}^{2N+1}(E-E_k)\right]^{1/2}}dE \\ &\qquad = 2\int_0^{\pi}\frac{E(z)^{m-1}}{\left[\prod_{\substack{k=1\\(k\neq 2j)\\(k\neq 2j+1)}}^{2N+1}[E(z)-E_k]\right]^{1/2}}dz . \end{aligned} \tag{A7}$$

(c) *Numerical integration algorithm.* To perform the integration a standard variable-step, fourth-order, combined Runge-Kutta and Adams-Moulton algorithm has been exploited [42]. Other integration approaches would probably work just as well.

2. Computing the eigenvalues $\{E_k\}$ from the amplitudes and commensurable wave numbers $\{A_j, k_j, E_1\}$

The mapping $\{A_j, k_j, E_1\} \rightarrow \{E_k\}$ defined by (A3) and (A4) implements the numerical procedure in Appendix A 3. Here the k_j are the wave numbers (assumed commensurable, $k_j = 2\pi j/L$), the amplitudes $A_j = 2\lambda a_j = E_{2j+1} - E_{2j}$, and E_1 is the reference energy. The true analytical inversion of (A3) (i.e., determine the $\{E_k\}$ given the matrix **C** or equivalently to determine $\{E_k\}$ from the $\{A_j, k_j, E_1\}$) is rather difficult analytically and I adopt a numerical method for this purpose. The procedure may be viewed as a numerical calculation beginning with $2N+1$ input eigenvalues values $\{E_k\}$ resulting in N values of $\{K_j\}$ and N values of $\{\omega_j\}$ (the one free parameter is the constant shift of all the $\{E_k\}$, which I refer to as E_{ref} following Ref. [24]). Other choices of input or output parameters are also possible; for instance one may choose to input instead $\{E_{\text{ref}}, A_j, G_j\}$ to get N values of the set $\{K_j, \omega_j\}$.

Numerical inversion. What follows is a Newton-Raphson search procedure for numerical inversion of the formulas that map DST into the Θ parameters $\eta_m(x,0)$. In this context the numerical inversion of a function into its N variables is performed as a gradient search of the function subjected to N constraints. In each case the function is calculated using the procedure of Appendix A 1, then a gradient iteration approach estimates the next value (approximate first derivatives are obtained by small variation of the "direct" input variables). This inversion procedure is found to work experimentally up to $N \sim 20$–30, but justification for its convergence is purely empirical.

3. Iterative determination of the $\{E_k\}$ given the amplitudes $\{A_j\}$ and the commensurable wave numbers $\{k_j\}$

For each j one defines the nonlinear mode amplitudes $A_j = E_{2j+1} - E_{2j}$ (the open bands in the Floquet diagram) and the $G_j = E_{2j} - E_{2j-1}$ (band-gap amplitudes) (2.7) and (2.8). Both A_j and G_j are always positive, since generally $E_{2j+1} > E_{2j}$. The reciprocal wave numbers $1/K_j$ (A4) are the N spatial periods of the hyperelliptic functions $\mu_j(x,0)$. Generally speaking the $1/K_j$ are not commensurable at the beginning of program execution; the end goal is to generate the commensurable set $\{K_j\}$ by iteration and hence to render the μ_j and $\eta(x,0)$ periodic functions. This is done by choosing the set $\{A_j, k_j, E_1\}$ as $N+1$ constant inputs [the wave numbers k_j are given by (2.3)] and the $\{G_j\}$ are N input initial values to be iterated upon in order to render the wave numbers commensurable, i.e., one seeks the convergence $\{K_j\} \rightarrow \{k_j\}$ during the iteration process.

At each iteration step (labeled "i") one computes

$$\{G_j^{(i)}, A_j E_1\} \rightarrow \{E_k^{(i)}\} .$$

The $\{E_k^{(1)}\} \rightarrow \{1/K_j^{(i)}\}$ are determined by the procedure in Appendix A 1. Each gap amplitude is varied $G_j^{(i)} \rightarrow G_j^{(i)} \delta G$ to evaluate the derivative matrix $D_{jm} = \partial(1/K_j^{(i)})/\partial G_m$. The iteration is made on the value of the band-gap amplitudes $G_j^{(i)}$,

$$G_j^{(i+1)} = G_j^{(i)} + \sum_{m=1}^{N} \left[\left[\frac{\partial(1/K_j^{(i)})}{\partial G_m} \right]_{jm}^{-1} \right] \times (1/K_m - 1/K_m^{(i)}) . \tag{A8}$$

If $G_j^{(i+1)} \geq 0$ then its value is left unchanged; otherwise one computes

$$G_j^{(i+1)} = \frac{G_j^{(i)}}{2} .$$

The end condition occurs when $|1 - |k_j/K_j^{(i)}|| < \epsilon$ for all j; the loop is repeated until this condition is met. The program parameters are ϵ and δG.

It is worth noting that the general wave-amplitude dependence in the dispersion relation of the Stokes expansion (A8) is also seen to occur in the more general dispersion relation (A4). This is clear because of the amplitude and wave-number dependence of the main spectrum $\{E_k\}$ as discussed in the above iterative approach.

APPENDIX B: NUMERICAL INTEGRATION OF THE SPATIAL DEPENDENCE OF THE HYPERELLIPTIC FUNCTIONS

In general the $\mu_j(x,0)$ are governed by strongly nonlinear, coupled equations (2.16), and as a result their numerical integration requires considerable concern [25,32]. Equations (2.16) depend upon $2N+1$ constants D_k which are obtained from the direct scattering problem as explained in Sec. II. The numerator in (2.16) may be viewed as a single-valued analytic function of μ_j on a two-sheeted Riemann surface. The argument of the square root in (2.16) has $2N+2$ branch points, one at infinity and $2N+1$ at $\mu_j = E_k$, where the argument goes to zero. All the E_k are real and just one μ_j lies in each "open band" so that consequently $E_{2j} \leq \mu_j \leq E_{2j+1}$ and the spatial derivatives of the μ_j are all real. Equations (2.16) are then conveniently written

$$\frac{d\mu_j}{dx} = 2\sigma_j \frac{\left[\prod_{k=1}^{2N+1} (E_k - \mu_j) \right]^{1/2}}{\prod_{\substack{i=1 \\ (i \neq j)}} (\mu_i - \mu_j)} , \tag{B1}$$

where the square root is now considered to be positive definite, and the constant $\sigma_j = \pm 1$ is an index representing the sign of the square root, i.e., which of the two Riemann sheets the derivative lies on. It is for this reason that I call the σ_j the "Riemann sheet indices." Note that

$$\operatorname{sgn}\left[\prod_{\substack{i=1\\(i\neq j)}}^{N}(\mu_i-\mu_j)\right]=(-1)^{j-1}\ . \tag{B2}$$

In the interval (E_{2j},E_{2j+1}) the μ_j must change monotonically while on a particular Riemann sheet. The μ_j change Riemann sheets exactly at a band edge, i.e., either E_{2j} or E_{2j+1}. When a μ_j reaches a band edge the derivative is exactly zero, $d\mu_j/dx=0$, and higher-order derivatives must be computed in any candidate for a numerical integrator.

To this end the spatial derivative of (B.1) is

$$\frac{d^2\mu_j}{dx^2}=-\mu_j'\sum_{\substack{m=1\\(m\neq j)}}^{N}\frac{\mu_j'-\mu_m'}{\mu_j-\mu_m}-\tfrac{1}{2}\sum_{p=1}^{2N+1}\frac{\mu_j'^2}{E_p-\mu_j}\ , \tag{B3}$$

where the primes denote spatial derivatives. The above expression is not particularly convenient for numerical analysis since the last sum includes a term that becomes indeterminate (zero over zero) whenever μ_j reaches a band edge. An equivalent form which is more convenient for numerical calculations is

$$\mu_j''=-\mu_j'\sum_{\substack{m=1\\(m\neq j)}}^{N}\frac{\mu_j'-\mu_m'}{\mu_j-\mu_m}-2\sum_{p=1}^{2N+1}\frac{\prod_{\substack{k=1\\(k\neq p)}}^{2N+1}(E_k-\mu_j)}{\prod_{\substack{i=1\\(i\neq j)}}^{N}(\mu_i-\mu_j)^2}\ . \tag{B4}$$

The numerical algorithm used herein is of second order and derives from a simple Taylor-series expansion of the hyperelliptic functions

$$\mu_j(x_{i+1})=\mu_j(x_i)+\frac{d\mu_j(x_i)}{dx}\Delta x+\frac{1}{2}\frac{d^2\mu_j(x_i)}{dx^2}(\Delta x)^2\ , \tag{B5}$$

where the first derivative is taken in the form (B.1) and the second derivative is given by (B.4). The algorithm has been programmed to be "automatic" in the sense that the spatial step Δx is varied to maintain a specified input precision; Δx is found to vary by about six orders of magnitude in order to ensure precise numerical control over the computation of the $\mu_j(x,0)$ for the most difficult case of N-soliton interactions.

[1] D. J. Korteweg and G. de Vries, Philos. Mag. Ser. **5**, 422 (1895).
[2] G. B. Whitham, *Linear and Nonlinear Waves* (Wiley, New York, 1974).
[3] J. Miles, Annu. Rev. Fluid. Mech. **12**, 11 (1980).
[4] D. J. Benny, J. Math. Phys. **45**, 52 (1966).
[5] R. R. Long, J. Atmos. Sci. **21**, 156 (1964).
[6] T. Maxworthy and L. G. Rededopp, Icarus **29**, 261 (1976).
[7] V. I. Karpman, *Nonlinear Waves in Dispersive Media* (Pergamon, Oxford, 1975).
[8] D. H. Peregrine, J. Fluid Mech. **25**, 321 (1966).
[9] F. Ursell, Proc. Cambridge Philos. Soc. **49**, 685 (1953).
[10] *Handbook of Mathematical Functions,* edited by M. Abramowitz and I. A. Stegun, Nat. Bur. Stand. Appl. Math. Ser. No. 55 (U.S. GPO, Washington, D.C., 1964).
[11] N. J. Zabusky and M. D. Kruskal, Phys. Rev. Lett. **15**, 240 (1965).
[12] C. S. Gardner, J. M. Greene, M. D. Kruskal, and R. M. Miura, Phys. Rev. Lett. **19**, 1095 (1967).
[13] V. E. Zakharov, S. V. Manakov, S.P. Novikov, and M. P. Pitayevsky, *Theory of Solitons. The Method of the Inverse Scattering Problem* (Nauka, Moscow, 1980) (in Russian).
[14] M. J. Ablowitz and H. Segur, *Solitons and the Inverse Scattering Transform* (SIAM, Philadelphia, 1981).
[15] R. K. Dodd, J.C. Eilbeck, J. D. Gibbon, and H. C. Morris, *Solitons and Nonlinear Wave Equations* (Academic, New York, 1982).
[16] A. C. Newell, *Solitons in Mathematics and Physics* (SIAM, Philadelphia, 1985).
[17] A. Degasperis, in *Nonlinear Topics in Ocean Physics,* edited by A. R. Osborne (Elsevier, Amsterdam, 1991), p. 701.
[18] A. R. Its and V. B. Matveev, Func. Anal. Appl. **9**, 65 (1975).
[19] E. Date and S. Tanaka, Prog. Theor. Phys. Suppl. **59**, 107 (1976).
[20] B. A. Dubrovin, V. B. Matveev, and S. P. Novikov, Russ. Math. Surveys **31**, 59 (1976).
[21] H. Flaschka and D. W. McLaughlin, Prog. Theor. Phys. **55**, 438 (1976).
[22] H. P. McKean and E. Trubowitz, Commun. Pure Appl. Math. **29**, 143 (1976).
[23] A. R. Osborne and L. Bergamasco, Nuovo Cimento B **85**, 229 (1985).
[24] A. R. Osborne and L. Bergamasco, Physica D **18**, 26 (1986).
[25] A. R. Osborne and E. Segre, Physica D **44**, 575 (1990).
[26] A. R. Osborne, in *Nonlinear Topics in Ocean Physics,* edited by A. R. Osborne (Elsevier, Amsterdam, 1991), p. 669.
[27] J. P. Boyd, J. Math. Phys. **25**, 3390 (1984a).
[28] J. P. Boyd, J. Math. Phys. **25**, 3402 (1984b).
[29] J. P. Boyd, J. Math. Phys. **25**, 3415 (1984c).
[30] J. P.Boyd and S. E. Haupt, in *Nonlinear Topics in Ocean Physics,* edited by A. R. Osborne (Elsevier, Amsterdam, 1991), p. 827.
[31] A. I. Bobenko and D. A. Kubenskii, Theor. Math. Phys. **72**, 929 (1987).
[32] A. R. Osborne (unpublished).
[33] A. R. Osborne, in *Soliton Theory: A Survey of Results,* edited by Allan P. Fordy (Manchester University Press, Manchester, 1989), pp. 152–173.
[34] A. R. Osborne, E. Segre, G. Boffetta, and L. Cavaleri, Phys. Rev. Lett. **67**, 592 (1991).
[35] A. R. Osborne and M. Petti, Phys. Rev. E **47**, 1035 (1993).
[36] E. R. Tracy, Ph.D. Thesis, University of Maryland, Plasma Report No. UMLPF 85-006, 1984 (unpublished).
[37] E. R. Tracy, H. H. Chen, and Y. C. Lee, Phys. Rev. Lett. **53**, 218 (1984).
[38] E. R. Tracy and H. H. Chen, Phys. Rev. A **37**, 815 (1988).
[39] A.R. Osborne, J. Comput. Phys. **94**, 284 (1991).
[40] W. E. Ferguson, Jr., H. Flaschka, and D. W. McLaughlin, J. Comput. Phys. **45**, 157 (1982).
[41] A. R. Its and V. B. Matveev, Func. Anal. Appl. **91**, 65 (1975).
[42] C. F. Gerald, *Applied Numerical Analysis* (Addison-Wesley, Reading, 1970).